Interaction of Nitrate, Barium, Strontium and Cadmium Ions with Fused Quartz/Water Interfaces Studied by Second Harmonic Generation

Patrick L. Hayes, Jessica N. Malin, Christopher T. Konek, and Franz M. Geiger*

Department of Chemistry, Northwestern University, 2145 Sheridan Road, Evanston, Illinois 60208

Received: August 30, 2007; In Final Form: November 3, 2007

Inorganic anions and cations are ubiquitous in environmental chemistry. Here, we use second harmonic generation to track the interaction of the environmentally important metal cations barium, strontium, and cadmium and the nitrate anion with fused quartz/water interfaces at pH 7. Using a dynamic flow system, we assess the extent of reversibility in the binding process and report the absolute number density of adsorbed cations, their charge densities, and their free energies of adsorption. We also present resonantly enhanced second harmonic generation experiments that show that nitrate is surface active and report the free energies and binding constants for the adsorption process. The second harmonic generation spectrum of surface-bound nitrate shows a new adsorption band that cuts further into the solar spectrum than nitrate in the aqueous or solid state. The results that we obtain for all four inorganic ions and the implications for tropospheric and aquatic chemistry as well as geochemistry are discussed in the context of fundamental science as well as pollutant transport models.

I. Introduction

A. Nitrate. The nitrate ion is commonly found in natural waters and in the atmosphere.[1,2] In natural waters, nitrate is an important nutrient, but excessive concentrations lead to eutrophication, and when in drinking water, it can be harmful to human health.[3,4] Anthropogenic sources of nitrate in the environment include agricultural fertilizers and NO_x emitted from combustion engines. Thus, it is not surprising that in recent work Nolan et al.[3] and Squillace et al.[4] reported that sources of drinking water regularly exceed the Environmental Protection Agency (US EPA) maximum contamination limit (MCL) of 10 ppm.[5] In the atmosphere, gas-phase nitrogen oxides represent a unique footprint left by human activity on a planetary scale[6] where they can undergo heterogeneous chemistry in presence of mineral dust or sea salt aerosols to produce adsorbed or particulate nitrates.[7,8]

In the atmosphere and in natural waters, irradiation of nitrate at its long wavelength absorption band (λ_{max} at approximately 300 nm) results in the photochemical production of important reactive species such as hydroxyl radicals and NO_x.[2,9,10] Thus, in fresh surface waters, nitrate can oxidize natural organic matter via hydroxyl radicals and impact aquatic redox chemistry.[10,11] In the atmosphere, the photochemical conversion of nitrate to NO_x has important implications for tropospheric ozone production because nitrogen dioxide can ultimately lead to ozone formation.[1,12] The photoactivity of nitrate depends on the wavelength and intensity of solar radiation reaching the Earth's surface. At wavelengths shorter than 320 nm, there is a steep drop-off in the solar radiation intensity reaching the Earth's surface, and radiation below 290 nm is completely adsorbed by stratospheric ozone.[1,13] Recently, Hudson et al. showed that the long wavelength absorption band of nitrate can shift to shorter wavelengths at high nitrate concentrations.[12] This effect is large enough to shift the absorbance peak maximum to wavelengths shorter than the ozone cutoff and thus has important implications for environmental nitrate photochemistry. These examples from geochemistry and atmospheric chemistry clearly indicate that it is important to consider the local environment of nitrate when evaluating its role in the atmosphere and natural waters.

Interfaces are ubiquitous in the environment, and because they provide a unique chemical medium for adsorbates they often play a key role in controlling the speciation, transport, and ultimate fate of environmentally important species. When dust plumes pass through clouds, water layers can condense on the individual particles,[14,15] creating an aqueous layer on the mineral surface were chemistry can occur. Nitrate is often found associated with mineral dust particles collected in different regions of the world,[15] and laboratory studies show that HNO_3 can undergo heterogeneous reactions on oxide surfaces in the presence of water.[15,16] In order to improve our understanding of how interfaces may influence nitrate chemistry, we use the nonlinear spectroscopic technique second harmonic generation (SHG)[17−19] to study nitrate at a mineral/water interface. Given the fact that silicates are the most common constituent in soil and mineral dust particles, we study the interaction of nitrate with fused quartz/water interfaces.[15] Although the fused quartz/water interface is clearly a pertinent model system for understanding the chemistry occurring on atmospheric mineral dust particles, this model system also provides valuable insight into heterogeneous geochemical environmental processes.

SHG is a powerful technique for studying heterogeneous systems because it can track adsorption and desorption processes in real-time, provide quantitative thermodynamic parameters via adsorption isotherms, and probe chemically specific electronic transitions of adsorbates with high surface selectivity.[17,20−29] Here we report spectroscopic studies of nitrate at the fused quartz/water interface to elucidate how the physics and chemistry of nitrate may be altered upon adsorption to a model mineral/water interface. We have already shown, through SHG studies, that electronic transitions of environmentally important species such as chromate(VI) or oxytetracycline can be perturbed

* To whom correspondence should be addressed. E-mail: geigerf@chem.northwestern.edu.

10.1021/jp076976g CCC: $40.75
Published on Web 01/09/2008

upon adsorption.[21,22] Given the sharp drop-off of solar radiation intensity at shorter wavelengths, a similar shift in the nitrate electronic transition at 300 nm could have important ramifications for nitrate photochemistry in natural waters and in the troposphere.

B. Barium, Strontium, and Cadmium. Similar to nitrate, cadmium is a well-known contaminant,[30,31] and its accumulation in soils has been linked to intensive agricultural activities.[32] One agricultural source of this metal is processed phosphate fertilizer from phosphate rock deposits.[33] The residual metal in the fertilizer represents a significant input of cadmium into the surrounding soils.[33] Other sources of cadmium include metal smelting and refining industries and leaching of landfills.[30] Cadmium is extremely toxic and has an extensive range of acute and chronic health effects including kidney damage, lung oedema, and osteoporosis.[31] Given the hazards associated with cadmium exposure the US EPA has set a MCL of 5 ppb for cadmium in drinking water.[30]

Barium is another divalent trace metal found in groundwater and other aquatic systems.[11] Although barium lacks the extreme toxicity of cadmium, it is of environmental interest because its anthropogenic sources include copper smelting, mining operations, and well drilling operations where it is directly released into the ground.[34,35] The US EPA has set an MCL of 2 ppm for barium.[34] Furthermore, the World Health Organization reported that health effects resulting from chronic exposure include hypertension, stroke, and kidney damage.[36] Barium and strontium, another alkaline earth metal, have environmentally important radioisotopes. Strontium-90 is a major fission product of uranium-235 and plutonium-239 with a half-life of 29.1 years, and is an important constituent of radioactive waste.[37] Radioactive strontium is metabolized in the body in the same way as calcium and thus accumulates in bones, leading to bone cancers and leukemia.[37] Strontium-90 and barium-140 are important radioactive species resulting from nuclear fallout.[38]

As with nitrate, surfaces and interfaces are expected to play a key role in the speciation, transportation, and ultimate fate of these environmentally important metal ions. Thus, their interaction with soil/water interfaces has been studied extensively. For instance, batch studies and titration experiments show that factors influencing cadmium adsorption to environmentally relevant interfaces include pH, soil organic content, and background electrolyte concentration.[39,40] Previous work on barium adsorption to mineral oxide interfaces such as iron oxides,[41,42] calcite,[43] alumina,[44] and quartz[45] has also shown a dependence on pH and background electrolyte. Similarly, it is known that strontium sorption to quartz depends on pH and background electrolyte.[46] After comparing the relative uptakes of several different alkaline earth ions at the quartz/water interface, Malati et al. suggested these ions bind through an outer-shell mechanism.[45]

Extended X-ray absorption fine structure (EXAFS) studies also provide valuable information regarding the local structure of an interfacial species. EXAFS studies have been carried out on cadmium sorbed to montmorillonite,[47] cryptomelane (KMn_8O_{16}),[48] goethite,[49] and hydrous ferric oxide.[50] These studies indicate Cd sorption can occur through outer-sphere complexation, inner-sphere complexation, or surface precipitation, and the exact mechanism of binding was reported to depend on the chemical identity of the substrate, the bulk solution pH, and the electrolyte and metal ion concentration. EXAFS studies have also been carried out on barium sorbed to montmorillonite and suggest a coexistence of outer- and inner-sphere surface complexes for sorbed Ba.[51]

To compliment this previous work, we utilize the nonlinear spectroscopy second harmonic generation (SHG) to study cadmium, barium, and strontium binding to the fused quartz/water interface. As with nitrate, SHG provides unique information regarding metal ion adsorption because of its ability to monitor the interaction of these metal ions with environmentally relevant interfaces in real-time, with surface-specificity and under flow conditions. Furthermore, we have already demonstrated that SHG can provide quantitative information regarding manganese(II) ion sorption to model environmental interfaces,[52] including absolute surface coverages. Herein, we expand upon our earlier work, and investigate the interfacial behavior of the environmentally important metal cations cadmium, barium, and strontium. To more accurately model natural waters, we have studied the sorption of these three metals from a 10 mM NaCl aqueous solution to mimic environmentally relevant ionic strengths. This concentration was selected because it lies in the upper range of ionic strengths for fresh water[2] and would also be relevant for regions where fresh waters mix with seawaters such as in marine estuaries. Although previous nonlinear optical studies have focused on dyes or chromophores with conjugated push−pull systems,[17,53,54] to our knowledge, this work represents the first time that the adsorption of alkaline earth and transition metal cations from electrolyte solutions has been studied using SHG. Furthermore, it is hoped that this work clearly demonstrates the unique versatility of SHG for studying a broad range of metal and nonmetal ions at environmental interfaces.

II. Theoretical Background

A. Resonantly Enhanced SHG. Second harmonic generation (SHG) is a nonlinear optical phenomenon, which can probe interfacial processes such as adsorption with high surface-selectivity.[17,19,25,55] SHG involves the conversion of two photons of an incident wavelength, ω, into an emitted photon of twice the frequency, 2ω. As can be seen below in eq 1, the intensity of the second harmonic response of an interface, I_{SHG}, is related to the second order nonlinear susceptibility, $\chi^{(2)}$, of the interface.[17] Furthermore, when the second harmonic generated at an interface matches an electronic resonance involving an interfacial species, the second-order susceptibility of the interface can be expressed as the sum of its non-resonant and resonant contributions, $\chi^{(2)}_{NR}$ and $\chi^{(2)}_{R}$.[56−58]

$$\sqrt{I_{SHG}} = E_{SHG} \propto \sqrt{|\chi^{(2)}|} = \sqrt{|\chi^{(2)}_{NR} + \chi^{(2)}_{R} e^{i\Delta\phi}|^2} \qquad (1)$$

The non-resonant and resonant contributions are linked through the phase factor, $\Delta\phi$. For resonantly enhanced SHG experiments, this phase difference is assumed to be 90°, which eliminates the cross product resulting from the square modulus.[23,27]

The resonant portion of the second-order susceptibility can be modeled as the product of the number density of a resonant adsorbate species, N_{ads}, and the second order molecular hyperpolarizability of that species, $\alpha^{(2)}$, averaged over all molecular orientations.[17,18]

$$\chi^{(2)}_{R} = N_{ads}\langle\vec{\alpha}^{(2)}\rangle \qquad (2)$$

From eqs 1 and 2, SHG can be used to probe the relative adsorbate surface coverage and to record adsorption isotherms, which yield important parameters such as thermodynamic binding constants and adsorption free energies. For SHG measurements of surface adsorbates, $\alpha^{(2)}$, can be expressed as

a summation of all of the electronic transitions of the adsorbate.[19,25,55]

$$\vec{\alpha}^{(2)}_{ijk} = \frac{-4\pi^2 e^3}{h^2} \sum_{b,c} \frac{< a|\vec{\mu}_i|b > < b|\vec{\mu}_j|c > < c|\vec{\mu}_k|a >}{(\omega - \omega_{ba} + i\Gamma_{ba})(2\omega - \omega_{ca} + i\Gamma_{ca})} \quad (3)$$

Here, *a*, *b*, and *c* represent the ground, intermediate, and excited electronic states, respectively, whereas ω_{ba} and ω_{ca} are the resonance frequencies of the corresponding electronic transitions. In addition, μ is the electric dipole moment operator, Γ_{ba} and Γ_{ca} are damping coefficients for each transition, *h* is Planck's constant, and *e* is the charge on an electron. From eq 3, it can be seen that when the incident frequency, ω, and/or the second harmonic frequency, 2ω, matches an electronic resonance within the adsorbate, the second-order molecular hyperpolarizability, $\alpha^{(2)}$, is increased. Following eqs 1 and 2, this increase in $\alpha^{(2)}$ results in the resonant enhancement of the overall SHG signal intensity. Resonance enhancement allows for interface-specific spectroscopic studies. Specifically for this work, nitrate displays a well-known electronic transition at 300 nm,[2,12] and therefore, resonantly enhanced SHG can be used to track the presence of nitrate at the fused quartz/water interface.

B. $\chi^{(3)}$ Technique. Resonantly enhanced SHG, although a powerful technique for studying adsorption,[21,26,28,29] is difficult to apply to metal ion adsorption at mineral oxide/water interfaces when the metal ion electronic transitions are either very weak or located in the far UV where water absorbs. To bypass this limitation we employ the $\chi^{(3)}$ technique as an alternative nonresonant SHG procedure.[59] In this technique, pioneered by Eisenthal and co-workers, the dependence of the SHG signal on interfacial potential, Φ_0, is modeled according to eq 4

$$\vec{E}_{2\omega} \propto \vec{\chi}^{(2)}\vec{E}_\omega\vec{E}_\omega + \vec{\chi}^{(3)}\vec{E}_\omega\vec{E}_\omega\Phi_0 \quad (4)$$

where $E_{2\omega}$ is the second harmonic electric field, E_ω is the applied fundamental electric field, and $\chi^{(2)}$ and $\chi^{(3)}$ are the second order and third order nonlinear susceptibilities of the interface.[60−62] Conceptually, eq 4 attributes the total SH light generated to two contributions. The $\chi^{(2)}$ term is independent of the static electric field and the corresponding electric potential at the fused quartz/water interface. In contrast, the $\chi^{(3)}$ term is modulated by the surface potential and is due, on the molecular-level, to the polarization and net orientation of water molecules that are aligned by an interfacial electric field resulting from a charged surface.[59,63] Specifically for this study, the fused quartz substrate carries a net negative surface charge density when in contact with pH 7 water and the resulting surface potential decays to the bulk value over a distance characterized by the Debye length, which, in turn, depends on electrolyte concentration.[2,64] The interfacial potential can be modeled using Gouy−Chapman theory

$$\Phi_0 = \frac{2k_B T}{ze} \operatorname{arcsinh}\left[\sigma\sqrt{\frac{\pi}{2\epsilon k_B T C_{\text{electrolyte}}}}\right] \quad (5)$$

where σ is the net surface charge density, *C* is the total concentration of electrolyte in the bulk aqueous solution, *z* is the charge of the screening electrolyte and ϵ is the permittivity of bulk water.[2,65] Equation 5 shows that changes in the surface potential, and thus the SHG E-field, depend on changes in charge density at the interface and also changes in the electrolyte concentration. By tracking the changes in the SHG signal that are caused by the interaction of Ba, Sr, and Cd cations with the mineral/water interface, we can study the molecular details of metal cation adsorption and desorption. Assuming Langmurian adsorption,[64,66,67] the surface charge density will be modulated by the bulk cation concentration according to the approach put forth by Salafsky and Eisenthal.[59]

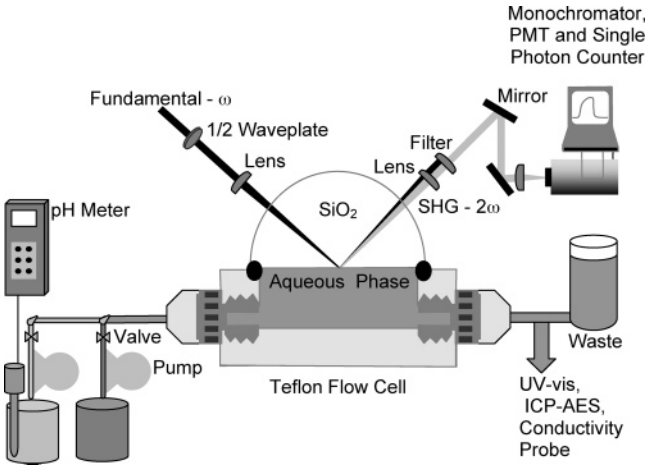

Figure 1. Experimental setup and flow cell used in SHG experiments. See experimental methods section for further details.

$$\sigma = \sigma_0 + \sigma_{\text{cation}}\left(\frac{K \times C_{\text{cation}}}{1 + K \times C_{\text{cation}}}\right) \quad (6)$$

In eq 6, σ_0 is the surface charge density of the bare fused quartz/water interface, σ_{cation} is the interfacial charge density resulting from adsorbed metal cations, *K* is the equilibrium binding constant for the cation, and *C* is the bulk cation concentration. Thus, by combining eqs 4−6, we obtain a model for the SHG signal intensity as a function of metal cation concentration. By fitting this model to our experimental data, we are able to determine quantitative information regarding metal ion adsorption, including binding constants, free energies of adsorption, the absolute number density of the metal cations at the interface, and information that is crucial to assessing the reversibility of metal cation binding to environmental interfaces. Together with the resonantly enhanced SHG measurements demonstrated in this work for the related inorganic anion, nitrate, SHG proves to be powerful for studying environmentally and biologically important anions and cations.

III. Experimental Methods

Our experimental setup has been described in detail previously.[20,21] Briefly, SHG studies were performed using a regeneratively amplified Ti:sapphire laser (Hurricane, Spectra Physics) pumping an optical parametric amplifier (OPA-CF, Spectra Physics) at a kHz repetition rate producing tunable light fields between 570 and 750 nm. The laser beam is directed through a variable density filter, where the power is attenuated to ~0.3 μJ per 120 fs pulse to safely avoid optical breakdown and nonlinear optical processes other than SHG. After focusing the attenuated fundamental probe light onto the fused quartz/water interface, the reflected fundamental and second harmonic light are passed through a UV-grade Schott filter and a monochromator to eliminate the fundamental before the second harmonic light is detected using a gated single photon counting system. The quadratic power dependence and appropriate bandwidth of the SHG signal are verified regularly to ensure that the sample damage threshold is not exceeded.

The experimental setup is pictured in Figure 1. A fused quartz hemispherical lens (ISP Optics) is clamped upon the open top

of a custom-built Teflon flow cell. A Viton O-ring is used to seal the lens to the flow cell and ensure that no leaks occur. Variable flow peristaltic pumps are used to pump Millipore water (18.2 MΩ) and aqueous analyte solutions of $NaNO_3$ (Fluka, 99%), $CdCl_2$ (Allied Chemical, 99%), $BaCl_2$ (Mallinckrodt, 99.9%), $SrCl_2$ (Acros Organics, 99%), and NaCl (VWR, 99%) through the flow cell. The flow rate is maintained at ∼1.0 mL/s. The pH of all water and analyte solutions is adjusted to 7 ± 0.2 through the use of HCl (VWR, ACS Reagent Grade) and NaOH (Spectrum Chemicals, 97%) solutions. All chemicals were used as received. (n.b. All solutions used were open to the atmosphere and approximately 0.1 mM NaOH was needed to neutralize the slight acidity due to dissolved CO_2. The added NaOH has a negligible effect on ionic strength in the metal studies because of the presence of 10 mM NaCl as a background electrolyte. In the case of nitrate, the combination of dissolved CO_2 and NaOH leads to an ionic strength of about 10^{-4} M for the water and nitrate solutions.)

Prior to each experiment, the fused quartz hemisphere was cleaned by treating its surface for 1 h with NoChromix (a chromium-free commercial glass cleaner, Godax Laboratories), followed by successive rinses of Millipore water and methanol. The lens was then sonicated in methanol for 6 min and dried for 30 min in an 80 °C oven. Finally, the lens was subjected to 30 s of plasma cleaning in air. Before placing the hemisphere in contact with the aqueous phase, the flow cell was cleaned by flowing 1 L of Millipore water through the entire flow cell system, including tubing.

To monitor the analyte concentration during experiments, aliquots from the output flow were collected. Nitrate concentrations were measured by monitoring the nitrate UV absorbance at 206 nm. At pH 7 and over the experimentally relevant nitrate concentrations (1×10^{-6}–6×10^{-5} M), the extinction coefficient at this wavelength was determined to be 6800 cm^{-1} M^{-1} (no added background electrolyte). Cadmium, barium and strontium concentrations were determined using Inductively Coupled Plasma Atomic Emission Spectroscopy (ICP-AES, Varian). NaCl concentrations were monitored using a conductivity meter (Fisher Traceable Conductivity and TDS Meter, Fisher Scientific).

IV. Results and Discussion

A. SHG Surface Spectroscopy. The SHG spectrum of nitrate adsorbed to the fused quartz/water interface was recorded, in triplicate, by monitoring the SHG signal as a function of the incident fundamental wavelength. The spectrum was collected using a 0.3 mM solution of sodium nitrate held at pH 7. This concentration corresponds to surface saturation of the nitrate anion (vide infra, section IV.C). Figure 2, which is a representative spectrum of the three recorded, shows that the SHG spectrum displays a maximum at 300 nm and a shoulder at longer wavelengths, which we observed in all of the three SHG spectra we recorded. This observed maximum matches the well-known λ_{max} observed for nitrate in aqueous systems, which may be attributed to the n−π* transition and/or the σ−π* transition as opposed to the π−π* transition, which occurs at ∼200 nm and which is much stronger.[2,12,68] In addition, Figure 2 includes the 10 mM aqueous and solid-state UV−vis spectra of sodium nitrate. The solid-state spectrum was collected by detecting the reflection of a UV−vis spectrometer light source from the surface of a pressed pellet of sodium nitrate using a fiber optic assembly. Both bulk spectra and the interfacial SHG spectra display the same λ_{max}.

Rotlevi and Treinen showed that the electronic transitions of nitrate can shift under different solvents conditions.[69] Additionally, Hudson et al. recently demonstrated that the λ_{max} of nitrate blue-shifts from 301 to 287 nm at high nitrate brine concentrations.[12] The shoulder near 330 nm that we observe in the SHG spectrum can be explained by considering that the bulk nitrate absorbance peak at 300 nm may be composed of several overlapping electronic transitions.[68] The energy and/or symmetry of one or more of these overlapping transitions may shift or be broken at the interface, which would result in the shoulder observed in the SHG spectrum. We note that, in contrast to the blue-shifted λ_{max} observed by Hudson et al. for nitrate brines, the shoulder observed in the SHG spectrum of surface-bound nitrate is red-shifted relative to the bulk absorbance. This difference suggests that when nitrate is localized at the fused quartz/water interface, the corresponding electronic transitions of nitrate are perturbed by a mechanism that is different from that operating in bulk brine solution. (For nitrate brines, it is believed that a loss of planar symmetry decreases conjugation resulting in higher energy transitions.[12]) Rotlevi and Treinin observed a red-shifted nitrate absorption band in solvents with low dielectric constants, and this solvent effect was attributed to reduced hydrogen-bonding capability.[69] Thus, the shoulder present in the SHG spectrum suggests that one of the transitions involved in the SHG resonance enhancement may be in a low-dielectric environment. At the molecular level, this low-dielectric environment would be consistent with the notion that solvent water molecules surround only a portion of the nitrate ion when it is adsorbed to the fused quartz/water interface. It should be noted that a similar effect was observed in our work on the adsorption oxytetracycline at the fused quartz/water interface.[22] Overall, the data presented here and those reported by Hudson et al. clearly testify to the rich electronic spectroscopy of nitrate in different geochemically and atmospherically important environments, which has been overlooked until now.

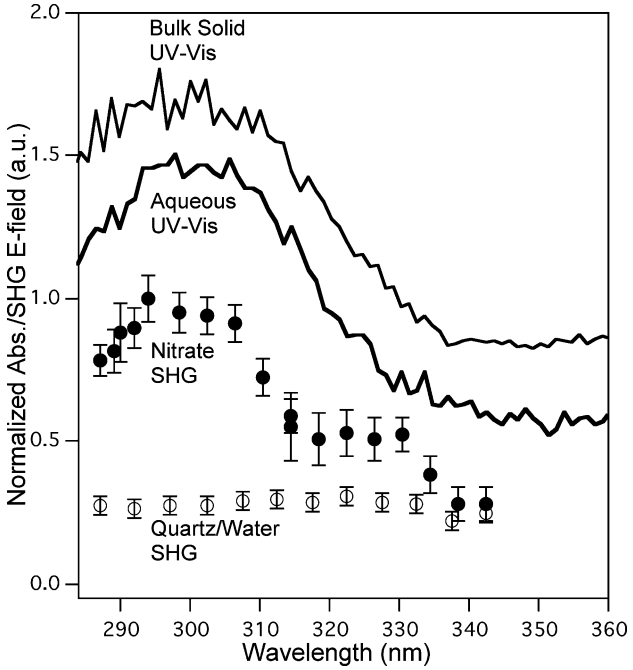

Figure 2. Nitrate SHG spectrum overlaid with the bulk aqueous and solid-state UV−vis spectra. Filled circles are the SHG spectrum of nitrate at the fused quartz/water interface at pH 7 and 0.3 mM concentration. Empty circles are the SHG response for the fused quartz/water interface in the absence of nitrate. All SHG data has been normalized to the maximum SHG E-Field value measured for nitrate. UV−vis spectra are individually normalized to one and offset for clarity.

B. Adsorption/Desorption Traces. To assess the reversibility of anion and cation binding to the interface, we performed

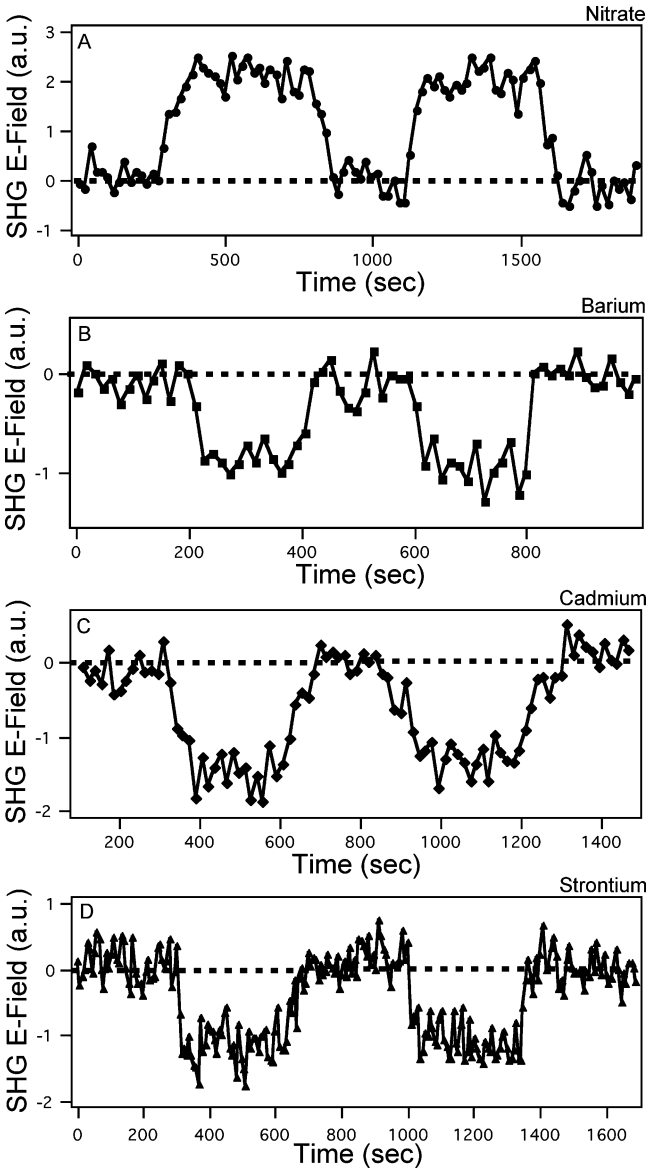

Figure 3. Adsorption/desorption traces for (from top) nitrate, barium, cadmium and strontium recorded at pH 7. Barium, cadmium and strontium traces were run at concentrations of 1, 2, and 4 mM, respectively, in the presence of 10 mM NaCl as a background electrolyte. The nitrate trace was measured at a bulk concentration of 0.5 mM without any background electrolyte. The dashed line indicates the background signal before introduction of the analyte.

adsorption/desorption studies at pH 7 by exposing fused quartz/water interfaces to aqueous nitrate, cadmium, barium, or strontium solutions in dynamic flow experiments. Using our dual-pump flow system, water is flowed past the quartz substrate while monitoring the interface with 600 nm laser light. At ~250 s, the water flow is stopped, and simultaneously, the analyte flow is started at the same flow rate such that the overall flow rate does not change. After this switch, the SHG signal for the interface in the presence of the analyte is monitored until it stabilizes, indicating steady-state conditions with respect to adsorption and desorption are met. At this time, the SHG signal is recorded for several minutes. We then replace the analyte flow with a flow of plain water while continuing the SHG signal collection until the baseline level is reached again.

The results of the adsorption/desorption experiments for nitrate, barium, cadmium, and strontium are shown in Figure 3. Figure 3 is obtained by taking the square root of the measured SHG intensity and then offsetting the data so that the background

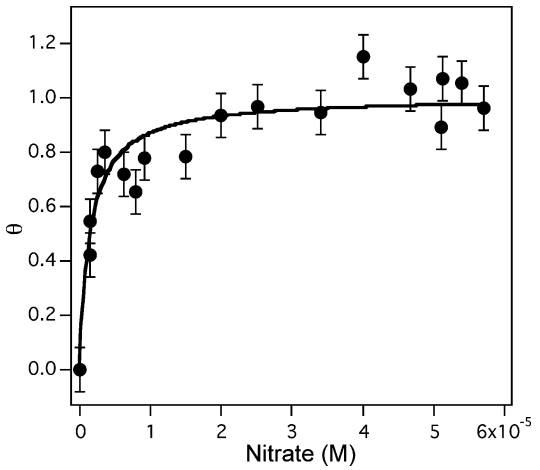

Figure 4. Isotherm for nitrate recorded at pH 7 and 298 K. The solid line represents the Langmuir model fit to the experimental data. The nitrate data is normalized to the saturated surface signal.

quartz/water signal corresponds to zero. For nitrate (Figure 3A), the fundamental laser wavelength is tuned to the 2-photon resonance observed in its SHG surface spectrum (300 nm). Thus, resonance enhancement is expected to occur with the SHG *E*-field increasing proportionally with interfacial nitrate number density (see eq 2). Indeed, an SHG E-field increase is observed when bulk aqueous nitrate is brought into contact with the interface, which indicates that nitrate adsorbs to the interface (i.e., that it is surface active). When the nitrate solution at the interface is replaced with water, the SHG E-Field decreases to the original baseline level. This indicates that the interaction is fully reversible. This result is consistent with field studies that have shown nitrate is readily transmitted through well-drained soils to groundwater.[3]

In contrast to the SHG signal increase from nitrate at the interface, we observe a signal decrease for barium, cadmium, and strontium (Figure 3, panels B−D, respectively) when these divalent bulk aqueous metal cations are brought into contact with the interface in the presence of 10 mM NaCl as a background electrolyte. This decrease is consistent with the $\chi^{(3)}$ effect as described in eqs 4 and 5. Similar to nitrate, the SHG E-field returns to the original baseline level when the metal ion solutions at the interface are replaced with plain water. This indicates that the interactions of these divalent cations with the fused quartz/water interface are fully reversible. The observed reversibility is consistent with field studies that show that barium becomes mobilized in higher salinity waters,[70] and laboratory studies that show that strontium and cadmium are only weakly bound by silicate minerals.[46,71]

C. Binding Curves for Nitrate, Barium, Cadmium, and Strontium. By plotting the SHG E-field as a function of bulk aqueous analyte concentration at pH 7, quantitative thermodynamic information regarding adsorption can be obtained.[59,64] After subtracting the nonresonant background using the proper phase relationships for resonantly enhanced SHG and normalizing to monolayer coverage,[27] a nitrate adsorption isotherm was obtained. Figure 4 shows that the interface becomes saturated with nitrate at a concentration of $\sim 2 \times 10^{-5}$ M. Additionally, we applied the Langmuir adsorption model to the isotherm data to obtain thermodynamic parameters for nitrate adsorption to the fused quartz/water interface. The fit yielded a binding constant, K_{ads}, of $7(1) \times 10^5$ M^{-1}. Using this binding constant, and a 55.5 M aqueous solution as the reference state,[64] we obtain a nitrate free energy of adsorption ($\Delta G_{ads,\ nitrate}$) of −43.3(4) kJ/mol, which is indicative of physisorption interactions medi-

ated by the hydrogen bonding and ion-dipole interactions that we expect for this aqueous/electrolyte system. It should be noted that nitrate is often considered inert and nonsorbing in geochemical studies.[72] However, using surface complexation modeling, Sahai and Sverjensky obtained binding constants ranging from 6.3×10^4 to 1.6×10^8 M^{-1} for nitrate adsorption to hematite, rutile, magnetite, and α-Al_2O_3.[73] The nitrate binding constant obtained using SHG is consistent with the binding constants determined by Sahai and Sverjensky, and it indicates that nitrate ions can be surface active.

A different approach is used for obtaining thermodynamic parameters for barium, strontium and cadmium interacting with fused quartz/water interfaces. As seen in Figure 5 and consistent with eqs 4 and 5, the SHG E-field decreases with increasing bulk barium, cadmium, and strontium concentrations when we record the corresponding binding curves. Similar to the adsorption/desorption traces, these binding curves were measured using 10 mM NaCl as the background electrolyte. Additionally, in Figure 5 the SHG response from increasing amounts of barium is contrasted against the SHG response from increasing amounts of NaCl added to a 10 mM NaCl solution. It can be seen that a NaCl solution that has the same ionic strength as a $BaCl_2$ solution leads only to a minimal change in SHG E-field relative to the change due to $BaCl_2$. Although the cadmium and strontium binding curves extend to a much higher analyte concentrations than for barium, it is still apparent from Figure 5 that at identical ionic strengths the divalent metals produce a much greater change in the SHG E-field than NaCl. This result indicates that the changes observed in the SHG E-Field for the three binding curves in Figure 5 are due interactions with the divalent metal cations and not due to the counterions or variation in the background electrolyte.

The fitting equation from which thermodynamic parameters can be extracted is obtained by combining eqs 4−6, and collecting constants.[59]

$$E_{\mathrm{SHG}} = A + B\,\mathrm{arcsinh}\left(\frac{30.2\,M^{1/2}m^2C^{-1}}{\sqrt{C_{\mathrm{electrolyte}}}} \times \left(\sigma_0 + \sigma_{\mathrm{cation}}\left(\frac{K \times C_{\mathrm{cation}}}{1 + K \times C_{\mathrm{cation}}}\right)\right)\right) \quad (7)$$

Above, A and B are fitting parameters composed of constants from eqs 4 and 5. The other two fitting parameters in eq 7 are K, the binding constant, and σ_{cation}, which is surface charge density due to the adsorbed metal ions. This fitting equation can be constrained by experimentally determining the surface charge density of the fused quartz/water interface in the absence of an adsorbate, σ_0. Following a procedure described by Eisenthal and co-workers,[61,63] SHG was used to measure a surface charge density of $-0.013(2)$ C/m^2 for the fused quartz/water interface (see Figure 6). When the surface charge density obtained is compared to literature values they are similar (within a factor of 5) for fused quartz/water interfaces near pH 7.[59,63]

Another challenge in fitting the data presented here is selecting the proper expression for the interfacial potential. Typically, the Gouy−Chapman model for symmetric electrolytes is utilized in the $\chi^{(3)}$ technique.[63,74,75] However, this model is not ideal for our experimental system given that the aqueous solution consists of a mixture of monovalent and divalent ions. While an analytical expression has been derived that relates the interfacial potential to the surface charge density and the electrolyte concentration for a 2:1:1 electrolyte solution such as those studied in this work,[76] the interfacial potential cannot be expressed in closed form for this case, which prevents its substitution into eq 4. To circumvent this problem, we approximate the potential using the Gouy−Chapman model for symmetric electrolytes, which provides the fitting equation described previously (eq 7).

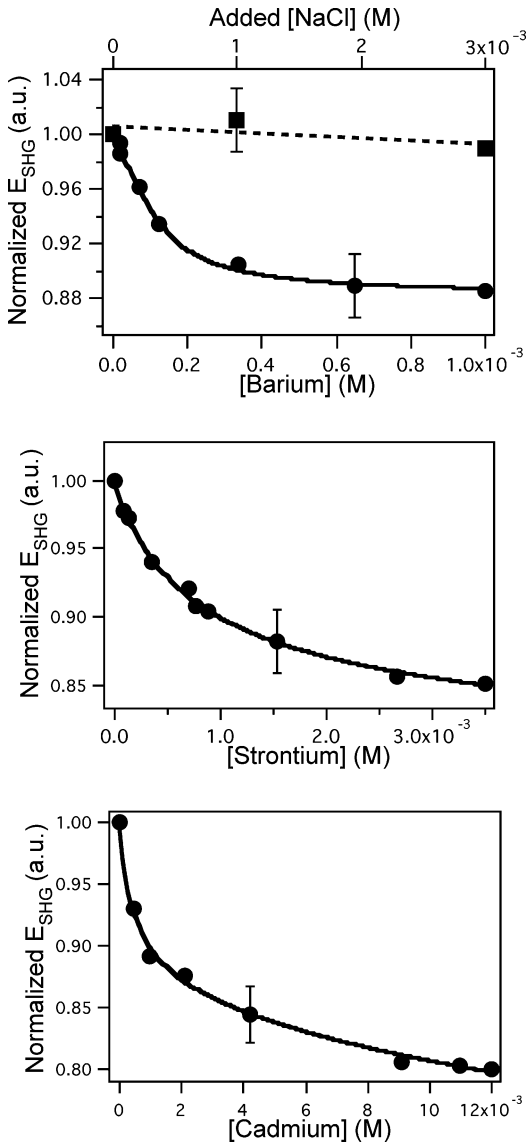

Figure 5. Binding curves for (from top) barium, strontium, and cadmium recorded at pH 7 and 298 K. The solid lines represent fits to the data using the $\chi^{(3)}$ equation modulated by the Gouy−Chapman model and the Langmuir model (eq 7). See text for further details regarding fits. Barium, strontium, and cadmium binding curves were measured using 10 mM NaCl as a background electrolyte. The barium, strontium, and cadmium curves are normalized to the background aqueous NaCl signal. Barium curve top axis: Solid squares represent the normalized SHG response for increasing concentrations of NaCl added to a 10 mM NaCl solution. The top axis, while spanning a different concentration range than the bottom axis, matches the ionic strengths resulting from the $BaCl_2$ concentrations displayed on the bottom axis. The dotted line represents a linear fit to the solid squares and illustrates the minimal change in SHG due to increasing NaCl over the relevant ionic strength range.

For barium and strontium, chemical equilibrium modeling software (ChemEQL, EAWAG: Swiss Federal Institute of Aquatic Science and Technology) indicates that the metal speciation is dominated by the 2+ state. On the basis of this information, we fit the experimental data using two different approaches. In the first approach, we assume that the screening that results from NaCl is negligible. We thus equate $C_{\mathrm{electrolyte}}$ with C_{cation}, which is equivalent to assuming that all the charge

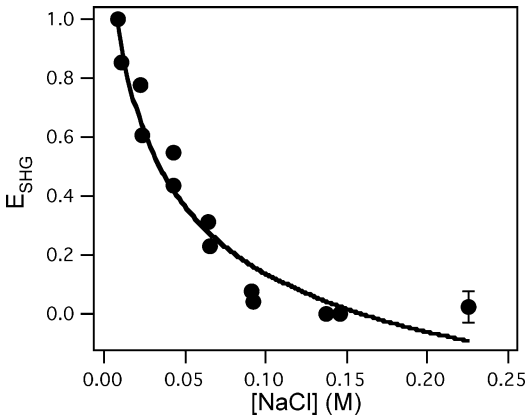

Figure 6. $\chi^{(3)}$ charge screening experiment for determination of charge density at the fused quartz/water interface. The line represents the fit of the Gouy−Chapman model to the experimental data. The data set is a combination of two experimental runs performed on separate days using freshly prepared fused quartz substrates (see text for details on substrate preparation). Data sets were combined by subtracting to shift the data sets so that the flat regions corresponded to a *y* axis value of zero and then normalizing to the data point corresponding to lowest NaCl concentration.

screening is due to the divalent cations. Increasing the divalent metal concentration in a pure water solution should have a stronger screening effect than increasing the divalent metal concentration in a pre-existing electrolyte solution. Thus, this first approach overestimates the change in SHG E-field that is attributable to the increasing screening electrolyte concentration, $C_{\text{electrolyte}}$. In the second approach we express $C_{\text{electrolyte}}$ as the sum of NaCl and analyte concentration, which is identical to assuming that $BaCl_2$ and $SrCl_2$ only dissociate to $BaCl^{1+}$ and $SrCl^{1+}$ in solution. This second approach underestimates the change that is attributable to the increasing screening electrolyte concentration because $BaCl^{1+}$ and $SrCl^{1+}$ will not screen the surface charge as effectively as the actual species in solution: Ba^{2+} and Sr^{2+}. We then report a range of values that spans the binding parameters obtained using these two fitting approaches. (It should be noted that in Figure 5 the fits to the binding curves represent the second approach were $C_{\text{electrolyte}}$ is the sum of the NaCl and analyte concentration.)

In contrast to barium and strontium, chemical equilibrium modeling indicates that cadmium, under the experimental conditions, has a more complicated bulk speciation and disassociates at appreciable concentrations into $CdCl^{1+}$ and Cd^{2+}. Fitting eq 7 to the cadmium binding curve data therefore requires that the total electrolyte concentration be modeled as the sum of the NaCl concentration and the $CdCl_2$ concentration. As before with the alkaline earth metals, this approach is equivalent to assuming that $CdCl_2$ only disassociates to $CdCl^{1+}$ in solution. From the equilibrium modeling, we know that under our experimental conditions a majority of $CdCl_2$ disassociates into $CdCl^{1+}$ and Cl^{1-} and not into Cd^{2+} and 2 Cl^{1-}. Dissociation into monovalent species becomes increasingly important at high $CdCl_2$ concentrations (51% at 1 mM $CdCl_2$ to 65% at 12 mM $CdCl_2$). At high cadmium and NaCl concentrations (12 and 10 mM, respectively), the number of divalent species represents less than 20% of the concentration of monovalent species. These considerations regarding cadmium speciation suggest that we can approximate $CdCl_2$ as a symmetric single-valent electrolyte, which would allow us to take the screening electrolyte concentration to be sum of the NaCl and $CdCl_2$ concentrations. In addition, we chose to fit the adsorption isotherm with a single effective binding constant in the Langmuir model since including more than one binding constant would introduce unreasonable error into our fitting through over-parametrization.

Following the procedure outlined above to fit the experimental data in Figure 5, binding constants ranging from 1.3(5)−4(1) $\times$ 10^4 M^{-1} and 2.3(3)−2.6(5) $\times$ 10^3 M^{-1} are obtained for barium and strontium, respectively. For cadmium, a binding constant of 2.9(8) $\times$ 10^3 M^{-1} is obtained. The corresponding free energies of adsorption, referenced to 55.5 M water, are found to range from −33(1) to −36.2(7) kJ/mol for barium and from −29.1(3) to −29.4(5) kJ/mol for strontium. The free energy for cadmium binding was calculated to be −29.7(8) kJ/mol. (See Table 1 for summary of parameters obtained from fitting the data in Figure 5). These values can be compared against analogous Langmuir isotherms obtained by classical batch techniques. Westrup et al. measured a binding constant of 3.0 $\times$ 10^3 M^{-1} for Cd(II) at the silica/water interface, which is (within error) equal to the binding constant reported in this paper.[77] The binding constant reported by Tsai et al., 5 $\times$ 10^3 M^{-1}, for Sr(II) at the bentonite/water interface[78] is slightly higher than the binding constant measured at the fused quartz/water interface using the $\chi^{(3)}$ technique. However, these two binding constants are within the same order of magnitude, and the discrepancy can be explained by the differing compositions of bentonite, which is an aluminosilicate mineral, and fused quartz.

Unlike resonantly enhanced SHG, the $\chi^{(3)}$ technique allows for the determination of the surface charge density at adsorbate saturation, and thus, the absolute number of adsorbates.[52,59] From the fitting equation we obtain an adsorbate surface charge density, σ_{cation}, ranging from 0.0135(7)−0.020(5) C/m^2 and 0.008(5)−0.014(1) C/m^2 for barium and strontium respectively, and 0.006(1) C/m^2 for adsorbed cadmium. Assuming that barium and strontium bind to the interface as +2 cations this charge density corresponds to 0.84(5)−1.3(4) $\times$ 10^{13} barium ions/cm^2 and 5(3)−8.8(7) $\times$ 10^{12} strontium ions/cm^2. For cadmium the charge density corresponds to 1.9(3) $\times$ 10^{12} Cd^{2+} ions/cm^2 or 3.8(6) $CdCl^{2+}$ ions/cm^2. Assuming hexagonally packed hard spheres and using the measured adsorbate densities, which range from 0.19−1.3 $\times$ 10^{13} ions/cm^2, we calculated adsorbate radii between 2−12 nm. However, the radii resulting from assuming hexagonal packing are significantly larger than literature values for the second-shell distances of the hydrated cations, which are approximately 480, 480, and 440 pm for barium, strontium, and cadmium, respectively.[79,80] Therefore, it appears that at maximum coverages the metal ions are not closely packed at the fused quartz/water interface, even when the second hydration sphere is considered. Instead, the fused quartz/water interface has a low density of surface-bound metal ions, which may be due to either the poor binding affinity of fused quartz or the background electrolyte competing for adsorption sites.

V. Conclusions and Environmental Implications

Adsorbed nitrate at the fused quartz/water interface was spectroscopically identified via resonantly enhanced SHG spectroscopy. The two-photon resonance near 300 nm is consistent with bulk aqueous and solid-state measurements. However, a shoulder at longer wavelengths is observed in the SHG spectrum of the adsorbed nitrate, and this feature is not present in the bulk spectra. Because the nitrate absorbance band is close to the cutoff of the solar spectrum in the troposphere at 290 nm, a perturbation of this band would alter the photochemical activity of nitrate in the environment. Therefore, the shoulder observed for nitrate at the fused quartz/water interface suggests that nitrate photoreactivity may be substantially different at mineral oxide/water interfaces as opposed to the bulk. Given

the fact that nitrate photolysis is an important source of reactive species in natural waters and the atmosphere, this change in reactivity has important environmental implications. Additionally, nitrate binding to the fused quartz/water interface was found to be completely reversible, to follow the Langmuir adsorption model, and to be driven by a free energy of adsorption of −43.3-(4) kJ/mol. These results are consistent with the general notion that nitrate is highly mobile in the environment.

SHG, specifically the $\chi^{(3)}$ method, was also utilized to study barium, strontium, and cadmium adsorption to the fused quartz/water interface under environmentally relevant background electrolyte concentrations. It was found that barium and cadmium adsorption in the presence of 10 mM NaCl is fully reversible with free energies ranging from −33(1) to −36.2(7) kJ/mol and −29.1(3) to −29.4(5) kJ/mol for barium and strontium, respectively. For cadmium, a free energy of −29.7-(8) kJ/mol was obtained. These free energies are several orders of magnitude lower than free energies that are expected for a binding mechanism in which the metal ion interacts directly with a negatively charged surface site through Coulombic attraction. Instead, they are more consistent with the formation of one or two hydrogen bonds upon adsorption.[65] The number density of metal ions at the fused quartz/water interface was also determined to be $0.84(5)-1.3(4) \times 10^{13}$ Ba ions/cm^2, $5(3)-8.8(7) \times 10^{12}$ Sr ions/cm^2, and $1.9(3) \times - 3.8(6) \times 10^{12}$ Cd ions/cm^2. These values are lower than what would be expected for hexagonally packed metal ions containing two hydration spheres ($\sim 1 \times 10^{14}$ ions/cm^2). Thus, when taken in combination, the free energies of adsorption and the low absorbate number densities indicate that barium, strontium, and cadmium ions are sparsely adsorbed to the fused quartz/water interface through an outer-shell mechanism. This result is in agreement with batch and EXAFS experiments that show barium and strontium bind to quartz and that cadmium binds to silicate minerals through an outer-shell mechanism.[45,46,71] This conclusion clearly demonstrates how the quantitative results from our SHG studies provide valuable mechanistic insight into metal cation adsorption at the mineral oxide/water interface.

The binding constants determined from fitting our adsorption isotherm data were also used to predict the environmental mobility of the four species studied in this work. The K_d model is used by regulatory agencies, including the US EPA, to calculate the extent to which pollution transport is slowed down in the environment due to heterogeneous binding events at solid/water interfaces.[81,82] To apply this model, we calculate a Langmuir adsorption isotherm using the binding constants determined from our experimental work. The K_d binding parameter is calculated from the simulated isotherm after converting surface coverage and bulk concentration to units of $g_{analyte}/g_{quartz}$ and g/mL, respectively.[20] (n.b. For barium, strontium, and cadmium we use the surface density determined in our experiments in carrying out this unit conversion. However, in the case of nitrate, a surface charge density of 5×10^{12} ions/cm^2 was assumed because this value falls in the range of those obtained for the cations.) A linear least-squares analysis of the submonolayer regime in the simulated adsorption isotherm then yields a slope, which is the K_d value in units of mL/g. The K_d value is then incorporated into an expression for the retardation factor, R_f.[82]

$$R_f = 1 + \frac{\rho}{n} K_d \tag{8}$$

Here, ρ is the bulk density of the soil, and n is its porosity. Given typical porosity values corresponding to unconsolidated granular deposits, ρ/n values for silica-rich soil environments range from 4 to 10 g/cm^3.[82] The limitations of this model have been discussed in our earlier work. However, the simplicity of K_d model allows us to calculate the R_f values for nitrate, barium, strontium and cadmium binding to the fused quartz/water interface at pH 7 (see Table 2 for summary of results). The range of R_f values calculated for nitrate was 1.032−1.08, which corresponds to nitrate traveling at 97%−93% the rate of groundwater. For the metal cations, due to the low K_d values all of the R_f values obtained were very close to unity. The K_d values obtained for Sr(II) and Cd(II) from the SHG experiments are substantially lower than literature values from batch experiments.[83] However, the discrepancy is not surprising given that the cited studies were run on soil samples taken from the field, instead of pristine fused quartz. After comparing our experimental results to batch studies, it appears that quartz is not the dominant adsorbent in many soil systems. Still, insofar as the results from our laboratory experiments are applicable to geochemical heterogeneous environments, the relatively low R_f values indicate that barium, strontium and cadmium will move through silica-rich environments at essentially the same rate as groundwater. By incorporating our SHG experiments into the K_d model, we have demonstrated the versatility of SHG for providing insight into the mobility and the mechanism of binding for a wide range of environmentally important ions.

TABLE 1: Summary of Binding Parameters for Nitrate, Barium, Strontium and Cadmium Adsorption to the Fused Quartz/Water Interface at pH 7 and 298 K

analyte	$-\Delta G_{ads}$ (kJ/mol)	K_{ads} (M^{-1})	adsorbate number density [ions/cm^2]
nitrate	43.3(4)	$7(1) \times 10^5$	−
barium[a]	33(1)−36.2(7)	$1.3(5)-4(1) \times 10^4$	$0.84(5)-1.3(4) \times 10^{13}$
strontium[a]	29.1(3)−29.4(5)	$2.3(3)-2.6(5) \times 10^3$	$5(3)-8.8(7) \times 10^{12}$
cadmium[a]	29.7(8)	$2.9(8) \times 10^3$	$1.9(3)-3.8(6) \times 10^{12}$

[a] Values correspond to measurements taken in 10 mM NaCl as a background electrolyte.

TABLE 2: Partition Coefficients and Corresponding Retardation Factor Values for Nitrate, Barium, Strontium, and Cadmium Binding to the Fused Quartz/Water Interface at pH 7

analyte	K_d (mL/g)	R_f
nitrate	0.008	1.032−1.08
barium[a]	0.0002−0.001	1.0008−1.01
strontium[a]	0.00002−0.00005	1.00008−1.0005
cadmium[a]	0.00001−0.00002	1.00005−1.0002

[a] Values correspond to measurements taken in 10 mM NaCl as a background electrolyte.

Acknowledgment. This work was supported by the Director, Chemical Sciences, Geosciences and Biosciences Division, of the U.S. Department of Energy under Grant No. DE-FG02-06ER15787 as well as the National Science Foundation Experimental Physical Chemistry program under grant no. CHE-0348873. Support from the DOE-funded Northwestern University Institute for Catalysis in Energy Processes and the Northwestern University International Institute for Nanotechnology is greatly appreciated. PLH acknowledges support from Schlumberger Oilfield Chemical Products. FMG is a Dow Chemical Company professor and a Sloan Fellow.

References and Notes

(1) Finlayson-Pitts, B. J.; Pitts, J. N. *Chemistry of the Upper and Lower Atmosphere: Theory, Experiments, and Applications*, 1st ed.; Academic Press: New York, 1999.

(2) Stumm, W.; Morgan, J. J. *Aquatic Chemistry, Chemical Equilibria and Rates in Natural Waters*, 3rd ed.; John Wiley & Sons: New York, 1996.

(3) Nolan, B. T.; Stoner, J. D. *Environ. Sci. Technol.* **2000**, *34*, 1156.
(4) Squillace, P. J.; Scott, J. C.; Moran, M. J.; Nolan, B. T.; Kolpin, D. W. *Environ. Sci. Technol.* **2002**, *36*, 1923.
(5) *Ground Water & Drinking Water, Consumer Factsheet on: Nitrates/Nitrites;* U.S. Environmental Protection Agency URL: http://www.epa.gov/safewater/contaminants/dw_contamfs/nitrates.html, Accessed: July 29th, 2007; Last Updated: November 28th, 2006.
(6) Richter, A.; Burrows, John, P.; Nuss, H.; Granier, C.; Niemeier, U. *Nature* **2005**, *437*, 129.
(7) Finlayson-Pitts, B. J. *Chem. Rev.* **2003**, *103*, 4801.
(8) Grassian, V. H. *Int. Rev. Phys. Chem.* **2001**, *20*, 467.
(9) Boxe, C. S.; Colussi, A. J.; Hoffmann, M. R.; Murphy, J. G.; Wooldridge, P. J.; Bertram, T. H.; Cohen, R. C. *J. Phys. Chem. A* **2005**, *109*, 8520.
(10) Zepp, R. G.; Hoigne, J.; Bader, H. *Environ. Sci. Technol.* **1987**, *21*, 443.
(11) Morel, F. M. M.; Hering, J. G. *Principles and Applications of Aquatic Chemistry*; John Wiley & Sons: New York, 1993.
(12) Hudson, P. K.; Schwarz, J.; Baltrusaitis, J.; Gibson, E. R.; Grassian, V. H. *J. Phys. Chem. A* **2007**, *111*, 544.
(13) Seinfeld, J. H.; Pandis, S. N. *Atmospheric Chemistry and Physics: From Air Pollution to Climate Change*; John Wiley & Sons: New York, 1998.
(14) Goodman, A. L.; Bernard, E. T.; Grassian, V. H. *J. Phys. Chem. A* **2001**, *105*, 6443.
(15) Usher, C. R.; Michel, A. E.; Grassian, V. H. *Chem. Rev.* **2003**, *103*, 4883.
(16) Rivera-Figueroa, A. M.; Sumner, A. L.; Finlayson-Pitts, B. J. *Environ. Sci. Technol.* **2003**, *37*, 548.
(17) Eisenthal, K. B. *Chem. Rev.* **1996**, *96*, 1343.
(18) Heinz, T. F. *"Second-Order Nonlinear Optical Effects at Surfaces and Interfaces," (Review Chapter) in Nonlinear Surface Electromagnetic Phenomena*; Elsevier: Amsterdam, 1991.
(19) Shen, Y. R. *The Principles of Nonlinear Optics*; John Wiley & Sons: New York, 1984.
(20) Mifflin, A. L.; Gerth, K. A.; Geiger, F. M. *J. Phys. Chem. A* **2003**, *107*, 9620.
(21) Mifflin, A. L.; Gerth, K. A.; Weiss, B. M.; Geiger, F. M. *J. Phys. Chem. A* **2003**, *107*, 6212.
(22) Mifflin, A. L.; Konek, C. T.; Geiger, F. M. *J. Phys. Chem. B* **2006**, *110*, 22577.
(23) Al-Abadleh, H. A.; Mifflin, A. L.; Musorrafiti, M. J.; Geiger, F. M. *J. Phys. Chem. B* **2005**, *109*, 16852.
(24) Al-Abadleh, H. A.; Mifflin, A. L.; Bertin, P. A.; Nguyen, S. T.; Geiger, F. M. *J. Phys. Chem. B* **2005**, *109*, 9691.
(25) Voges, A. B.; Al-Abadleh, H. A.; Geiger, F. M. Development of Nonlinear Optical Spectroscopies for Studying Heterogeneous Environmental Catalytic Processes. In *Environmental Catalysis*; CRC Press: Boca Raton, FL, 2005.
(26) Hayes, P. L.; Gibbs-Davis, J. M.; Musorrafiti, M. J.; Mifflin, A. L.; Scheidt, K. A.; Geiger, F. M. *J. Phys. Chem. C* **2007**, *111*, 8796.
(27) Mifflin, A. L.; Musorrafiti, M. J.; Konek, C. T.; Geiger, F. M. *J. Phys. Chem. B* **2005**, *109*, 24386.
(28) Gibbs-Davis, J. M.; Hayes, P. L.; Scheidt, K. A.; Geiger, F. M. *J. Am. Chem. Soc.* **2007**, *129*, 7175.
(29) Konek, C. T.; Illg, K. D.; Al-Abadleh, H. A.; Voges, A. B.; Yin, G.; Musorrafiti, M. J.; Schmidt, C. M.; Geiger, F. M. *J. Am. Chem. Soc.* **2005**, *127*, 15771.
(30) *Ground Water & Drinking Water, Consumer Factsheet on: Cadmium;* U.S. Environmental Protection Agency URL: http://www.epa.gov/safewater/dwh/c-ioc/cadmium.html; Accessed: July 30th, 2007; Last Updated: November 28th, 2006.
(31) Sterner, O. *Chemistry, Health and Environment*; Wiley-VCH: New York, 1999.
(32) Chen, W.; Chang, A. C.; Wu, L. *Ecotox. Environ. Safe.* **2007**, *67*, 48.
(33) McBride, M. B.; Spiers, G. *Commun. Soil. Sci. Plan.* **2001**, *32*, 139.
(34) *Ground Water & Drinking Water, Consumer Factsheet on: Barium;* U.S. Environmental Protection Agency URL: http://www.epa.gov/safewater/contaminants/dw_contamfs/barium.html; Accessed: July 30th, 2007; Last Updated: November 28th, 2006.
(35) Shock, S. S.; Bessinger, B. A.; Lowney, Y. W.; Clark, J. L. *Environ. Sci. Technol.* **2007**, *41*, 4813.
(36) Fawell, J. K.; Mascarenhas, R. *Barium in Drinking-water: Background document for developments of WHO Guidelines for Drinking-water Quality*, World Health Organization, 2004 http://www.who.int/water_sanitation_health/dwq/chemicals/barium.pdf.
(37) Makhijani, A. *Chem. Eng. News.* **2003**, *81*, 100.
(38) Cosma, C. *J. Radioanal. Nucl. Ch.* **2002**, *251*, 221.
(39) Lee, S.-Z.; Allen, H. E.; Huang, C. P.; Sparks, D. L.; Sanders, P. F.; Peijnenburg, W. J. G. M. *Environ. Sci. Technol.* **1996**, *30*, 3418.
(40) Prelot, B.; Janusz, W.; Thomas, F.; Villieras, F.; Charmas, R.; Piasecki, W.; Rudzinski, W. *Appl. Surf. Sci.* **2002**, *196*, 322.
(41) Kurbatov, J. D.; Kulp, J. L.; Mack, E., Jr. *J. Am. Chem. Soc.* **1945**, *67*, 1923.
(42) Kurbatov, M. H. *J. Am. Chem. Soc.* **1949**, *71*, 858.
(43) Douglas, H. W.; Walker, R. A. *T. Faraday. Soc.* **1950**, *46*, 559.
(44) Lowson, R. T.; Evans, J. V. *Aust. J. Chem.* **1984**, *37*, 2165.
(45) Malati, M. A.; Estefan, S. F. *J. Colloid. Interf. Sci.* **1966**, *22*, 306.
(46) Chen, C.-C.; Coleman, M. L.; Katz, L. E. *Environ. Sci. Technol.* **2006**, *40*, 142.
(47) Takamatsu, R.; Asakura, K.; Chun, W.-J.; Miyazaki, T.; Nakano, M. *Chem. Lett.* **2006**, *35*, 224.
(48) Randall, S. R.; Sherman, D. M.; Ragnarsdottir, K. V. *Chem. Geol.* **1998**, *151*, 95.
(49) Collins, C. R.; Ragnarsdottir, K. V.; Sherman, D. M. *Geochim. Cosmochim. Acta* **1999**, *63*, 2989.
(50) Spadini, L.; Manceau, A.; Schindler, P. W.; Charlet, L. *J. Colloid Interface Sci.* **1994**, *168*, 73.
(51) Zhang, P. C.; Brady, P. V.; Arthur, S. E.; Zhou, W. Q.; Sawyer, D.; Hesterberg, D. A. *Colloid Surf. A* **2001**, *190*, 239.
(52) Konek, C. T.; Musorrafiti, M. J.; Voges, A. B.; Geiger, F. M. Tracking the Interaction of Transition Metal Ions with Environmental Interfaces Using Second Harmonic Generation. In *Adsorption of Metals by Geomedia II*; Elsevier, in press, 2007.
(53) Steel, W. H.; Walker, R. A. *Nature* **2003**, *424*, 296.
(54) Corn, R. M.; Higgins, D. A. *Chem. Rev.* **1994**, *94*, 107.
(55) Boyd, R. W. *Nonlinear Optics*, 2nd ed.; Academic Press: New York, 2003.
(56) Petersen, P. B.; Johnson, J. C.; Knutsen, K. P.; Saykally, R. J. *Chem. Phys. Lett.* **2004**, *397*, 46.
(57) Wang, H.; Borguet, E.; Eisenthal, K. B. *J. Phys. Chem. A* **1997**, *101*, 713.
(58) Yam, R.; Berkovic, G. *Langmuir* **1993**, *9*, 2109.
(59) Salafsky, J. S.; Eisenthal, K. B. *J. Phys. Chem. B* **2000**, *104*, 7752.
(60) Xiao, X. D.; Vogel, V.; Shen, Y. R. *Chem. Phys. Lett.* **1989**, *163*, 555.
(61) Yan, E. C. Y.; Liu, Y.; Eisenthal, K. B. *J. Phys. Chem. B* **1998**, *102*, 6331.
(62) Zhao, X.; Ong, S.; Wang, H.; Eisenthal, K. B. *Chem. Phys. Lett.* **1993**, *214*, 203.
(63) Ong, S.; Zhao, X.; Eisenthal, K. B. *Chem. Phys. Lett.* **1992**, *191*, 327.
(64) Adamson, A. W. *Physical Chemistry of Surfaces*, 5th ed.; John Wiley & Sons: New York, 1990.
(65) Atkins, P.; de Paula, J. *Physical Chemistry*, 7th ed.; W. H. Freeman and Company: New York, 2002.
(66) Masel, R. I. *Principles of Adsorption and Reaction on Solid Surfaces*; John Wiley & Sons: New York, 1996.
(67) Somorjai, G. A. *Introduction to Surface Chemistry and Catalysis*; John Wiley & Sons: New York, 1994.
(68) Maria, H. J.; McDonald, J. R.; McGlynn, S. P. *J. Am. Chem. Soc.* **1973**, *95*, 1050.
(69) Rotlevi, E.; Treinin, A. *J. Phys. Chem.* **1965**, *69*, 2645.
(70) Shaw, T. J.; Moore, W. S.; Kloepfer, J.; Sochaski, M. A. *Geochim. Cosmochim. Acta* **1998**, *62*, 3047.
(71) Farquhar, M. L.; Vaughan, D. J.; Hughes, C. R.; Charnock, J. M.; England, K. E. R. *Geochim. Cosmochim. Acta* **1997**, *61*, 3051.
(72) Dzombak, D. A.; Morel, F. M. M. *Surface Complexation Modeling, Hydrous Ferric Oxide*; John Wiley & Sons: New York, 1990.
(73) Sahai, N.; Sverjensky, D. A. *Geochim. Cosmochim. Acta* **1997**, *61*, 2801.
(74) Boman, F. C.; Musorrafiti, M. J.; Gibbs, J. M.; Stepp, B. R.; Salazar, A. M.; Nguyen, S. T.; Geiger, F. M. *J. Am. Chem. Soc.* **2005**, *127*, 15368.
(75) Konek, C. T.; Musorrafiti, M. J.; Al-Abadleh, H. A.; Bertin, P. A.; Nguyen, S. T.; Geiger, F. M. *J. Am. Chem. Soc.* **2004**, *126*, 11754.
(76) Abraham-Shrauner, B. *J. Colloid. Interf. Sci.* **1975**, *53*, 496.
(77) Westrup, J. L.; Fritzen, M. B.; Souza, A. J.; Bedendo, G. C.; Nome, F.; Fiedler, H. D. *J. Brazil. Chem. Soc.* **2005**, *16*, 982.
(78) Tsai, S.-C.; Juang, K.-W. *J. Radioanal. Nucl. Ch.* **2000**, *243*, 741.
(79) Ohtaki, H.; Radnai, T. *Chem. Rev.* **1993**, *93*, 1157.
(80) Richens, D. T. *The Chemistry of Aqua Ions*; John Wiley & Sons: New York, 1997.
(81) *Understanding Variation in Partition Coefficient, Kd, Values: Introduction;* United States Environmental Protection Agency www.epa.gov/radiation/cleanup/partition.htm; Accessed: April 1st, 2007; Last Updated: May 16th, 2006.
(82) Langmuir, D. *Aqueous Environmental Geochemistry*; Prentice Hall, Inc: New Jersey, 1997.
(83) *Understanding variation in partition coefficient, Kd, Values. Volume II: Review of geochemistry and available Kd values for cadmium, cesium, chromium, lead, plutonium, radon, strontium, thorium, tritium (3H), and uranium,* EPA402-R-99-004B; United States Environmental Protection Agency, 1999 http://nepis.epa.gov/EPA/html/Pubs/pubtitleOAR.htm.